

Deep learning modelling of manufacturing and build variations on multi-stage axial compressors aerodynamics

Giuseppe Bruni^{a,b,*}, Sepehr Maleki^b, Senthil K. Krishnababu^{a,b}

^aSiemens Energy, 1 Waterside South, Lincoln, LN5 7FD, United Kingdom

^bUniversity of Lincoln, Brayford Way, Lincoln, LN6 7DL, United Kingdom

Abstract

Application of deep learning methods to physical simulations such as CFD (Computational Fluid Dynamics) for turbomachinery applications, have been so far of limited industrial relevance. This paper demonstrates the development and application of a deep learning framework for real-time predictions of the impact of manufacturing and build variations, such as tip clearance and surface roughness, on the flow field and aerodynamic performance of multi-stage axial compressors in gas turbines. The associated scatter in compressor efficiency is known to have a significant impact on the corresponding overall performance and CO_2 emissions of the gas turbine, therefore posing a challenge of great industrial and environmental relevance. The proposed architecture is proven to achieve an accuracy comparable to that of the CFD benchmark, in real-time, for an industrially relevant application. The deployed model, is readily integrated within the manufacturing and build process of gas turbines, thus providing the opportunity to analytically assess the impact on performance and potentially reduce requirements for expensive physical tests.

Keywords:

Convolutional Neural Network, Deep Learning, Aerodynamics, Axial Compressor, CFD, Gas Turbine.

1. Introduction

Gas turbine manufacturers have gathered vast amount of operational data over the years, enabling them to establish best practices and design guidelines for their manufacturing and build processes. These guidelines, often consider a trade-off between product cost and engine performance, with tolerance ranges specified accordingly. However, the impact on performance used to define these ranges is typically based on previous experience and simplified correlations. Significant advancements in accuracy and computational cost, have also made CFD analyses an integral part of industrial design processes of turbomachinery components. Despite these advances, analytical models are generally limited to simplified scenarios (not considering real-world effects). Build-specific CFD models have been demonstrated to provide excellent agreement with test data [1], but are not traditionally used as part of the manufacturing and build process as a day-to-day occurrence, due to the associated computational cost and requirement for specialized engineers to carry out the analyses. The proposed deep learning framework aims to model the effect of manufacturing and build variations on engine performance, achieving similar accuracies to standard CFD solvers, in a significantly shorter timescale. The focus of the current work is on tip clearance and surface roughness variations, two of the main sources of performance variability, but the framework is readily generalisable to other manufacturing variations. This is incorporated into the manufacturing and build process, providing instantaneous feedback, which can potentially be used to reduce the requirements for expensive physical testing when clearances go outside the acceptance limits.

The challenge: The impact of manufacturing and build variations on the overall performance of gas turbines is known to be significant [2] [3], with the axial compressor, as shown in Figure 1, being a large contributor. For a given design, compressor efficiency is affected by a combination of in-tolerance variations, which can lead to a substantial

*Corresponding author

Email address: giuseppe.bruni@siemens-energy.com (Giuseppe Bruni)

increase in CO_2 emissions compared to the design target. The aerodynamic performance of multi-stage axial compressors is predicted as standard practice using CFD (Computational Fluid Dynamics). However, these calculations are traditionally performed only for a simplified "as designed" geometry, that differs from the specific build of each engine. Therefore, accurately predicting the performance of each engine build by modelling the impact of manufacturing and build variations on engine performance within a short timescale is of great industrial and environmental importance.

Our contribution: This work demonstrates the application of a novel deep learning framework previously developed by the authors [4] for predicting the impact of manufacturing and build variations on the flow field and overall performance of a multi-stage axial compressors in real-time. Our proposed methodology achieves accuracy levels similar to those of a standard CFD solvers, within a significantly shorter timescale. This work extends the architecture first introduced in previous work by the authors [4], from a proof of concept to a significantly more complex and computationally expensive application of great industrial relevance, demonstrating the aim to provide a generalisable framework. This is then proven to be readily integrated into the manufacturing and build process, providing the capability to model each engine build. In addition to avoiding the computational costs, long lead times, and specialized personnel requirements of traditional CFD analyses, it can be used to potentially reduce expensive physical tests.

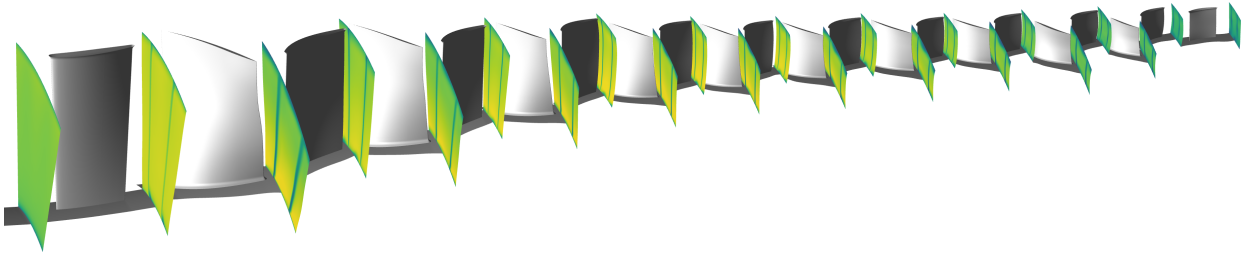


Figure 1: Overview of the CFD domain and axial velocity contours at the mixing-plane locations

1.1. Tip Clearance variation background

Several manufacturing and build variations affect the overall performance of axial compressors, including tip clearance variations which are one of the main contributors [2] [3]. The term tip clearance refers to the radial distance between the stationary and rotating components within the compressor, such as the rotor blades and casing, or stator blades and rotor hub. Generally, the tip clearance must be large enough to prevent rubbing during operation, but small enough to avoid excessive aerodynamic losses. Axial compressors are designed to operate at a defined tip clearance, which can vary across stages. During manufacturing, the "cold clearance" is specified and measured as part of the build process in stationary conditions. However, during operation, the "hot clearance" can be significantly smaller due to thermal expansion and centrifugal effects. The cold clearance values have a target value and tolerance range, set by gas turbine manufacturers, based on trade-offs between undesirable rubbing and minimizing tip leakage losses. For a given "cold clearance", the corresponding "hot clearance" can be calculated using either analytical models or operational experience. The "hot clearance" is the actual clearance found during operation, and therefore is used in the CFD and machine learning models presented in this paper. The aerodynamic mechanisms driving tip leakage flows have been extensively researched over the years [5] and can be modeled analytically with varying degrees of fidelity. Steady-state single passage CFD calculations are often used to model the effects of tip clearance variations on overall performance [6], and are used as ground-truth for this study. Non-axisymmetric tip clearance variations are known to affect the overall performance and surge margin [7] and can be relevant for in-service degradation. However, for manufacturing variations they can be neglected [4] and single passage models can be used for the analyses.

1.2. Surface roughness variation background

CFD analyses traditionally assume aerofoil and gas path surfaces to be aerodynamically smooth. This assumption is often not valid for production components, which have a non-negligible roughness due to coating selection or manufacturing methods. A trade-off can be identified between production cost and roughness, as smoother finishes tend to be progressively more expensive. Therefore, it is of paramount importance to be able to characterize the impact

of different surface roughness levels on the aerodynamic performance. This is particularly relevant when comparing test data from different builds with coating from different suppliers, as they can potentially have significantly different roughness. Experimental work has shown that increased roughness on the aerofoil surface has a detrimental effect on efficiency. One possible way to describe the surface roughness is to consider the average R_a for each blade row, which can be measured for a given set of blades. The R_a can then be converted to an equivalent sand grain roughness to be used for CFD using the equation $k_s = 5.2 \cdot R_a$. More details on surface roughness modelling for CFD predictions is provided by the authors in previous work [1].

1.3. Machine Learning applications to turbomachinery

In recent years, there has been a significant amount of research into the utilization of machine learning techniques for turbomachinery applications. These include predicting the aerodynamic performance due to tip clearance variations [8] and design modifications [9], as well as aeromechanic predictions for both forced response [10] and flutter [11]. As often the output variables are predicted directly from the input variables with a "black box" approach, these methodologies have varying degrees of accuracy and generalisability, depending on the complexity of the application. However, the ability to accurately predict variations in target variables for turbomachinery in a manner that is both reliable and generalisable, is contingent upon the accuracy of flow field predictions. It is only through precise flow field predictions that the overall performance figure of interest can be calculated through the application of relevant physical equations that govern the dynamics. The potential benefits of using machine learning approaches for predicting full flow fields, have been demonstrated in some simplified cases in literature for 2D aerofoils on both cartesian [12][13][14] and unstructured [15] grids. Li et. al. [16], using CNNs to predict the flow field downstream of a single fan row, which was then used for noise predictions applications. A similar approach was used also by Rao et. al. [17] for the semantic segmentation of an aero-engine intake using U-Net and U-Net++ architectures. Graph neural networks [18] [19] have also been applied to 3D turbomachinery, with a single row compressor [20] and turbine [21], which suggested potential challenges related to scalability and practicality for industrial applications. For instance, the computational cost associated with training, and the size of the required model, make the approach impractical for multi-stage compressors. These applications typically use computational meshes in the order of magnitude of 10 million nodes. Furthermore, storing the CFD data required for training and future simulations would require several petabytes, for a typical engine manufacturer, which is not practical. Purely data-driven approaches typical of supervised learning require large amount of data, so that the network can learn the solution manifold. A recent review [22] has highlighted the potential of other approaches to mitigate these issues such as Physics-Informed Neural Networks (PINNs), Reinforcement Learning (RL), and Generative Adversarial Networks (GANs) [23]. However, none of those methods can currently provide accurate, generalisable and scalable solutions to complex 3D turbomachinery applications.

1.4. Novel solution to machine learning scalability

To address these challenges, we introduce a pre-processing step to extract only the relevant engineering data from the computational domain, such as blade-to-blade planes, blade surfaces, axial cuts, loading distributions, radial distributions, stage-wise performance, and overall performance. In most cases, these provide sufficient information to the aerodynamicist for design and analyses activities, while close examination of the 3D flow field of a CFD solution is generally only necessary in non-standard cases. Once the relevant engineering data has been extracted from the computational domain, it can be interpolated onto a simplified grid with a resolution that is deemed acceptable for the application in question. Only selected fundamental variables are predicted, while the derived ones can be computed using the appropriate physical equations, significantly reducing the computational cost without sacrificing accuracy, as only the necessary data required to calculate the target variables is retained. Targeting the flow field predictions and using the relevant physical equations to calculate the corresponding overall performance renders the methodology generalisable, while filtering only relevant parts of the CFD solution makes the methodology scalable to complex industrial applications. This was first introduced by the authors in a previous work for a single stage compressor application [4], and is now extended to a multi-stage compressor application, with a computational domain one order of magnitude larger. This paper demonstrates that the framework developed in the previous paper can be translated from an academic test case, to a complex real-world application with significant engineering relevance.

2. Methodology

A modern multi-stage industrial axial compressor consisting of 10 stages, as shown in Figure 1, is considered in this work. Each stage is comprised by a row of rotor blades and a row of stator blades with a given blade count. The effect of tip clearance and surface roughness variations on each blade row are the focus of this study. Future work will include other manufacturing and build variations such as geometry variations, as well as different operating conditions.

2.1. Data Generation

The ground-truth data used for training are the CFD results for the configuration of interest. This computational model consisted of a single passage model of the 10 stages, with mixing plane interfaces. The computational mesh was generated using Numeca AUTOGRID5, and the CFD solver used was Trace, with SST $K - \omega$ turbulence model. More details on the computational setup used have been provided in previous publications [10]. The development of build-specific CFD models for compressor aerodynamic predictions and its validation against engine test data was also presented in previous work by the authors, discussing the relative effects of various manufacturing and build variations [1]. The tip clearance and surface roughness were varied for each row (I1=IGV, R1=Rotor-1, S1=Stator-1, etc.) within out-of-tolerance conditions up to 50% larger and tighter than the drawing specifications, as shown in Figure 2. This range is significantly larger than the tolerance typically specified for gas turbine applications, and was selected to demonstrate the robustness of the methodology to out-of-tolerance cases. The input variable space was sampled using latin-hypercubic sampling. The dataset generated for this study comprises 400 CFD solutions, each of which was executed using automated and parallelized processes, taking 90 minutes on 72 CPUs for each case. Even if the computational cost required to generate the dataset for supervised training is potentially high, it should be noted that most of the data is already available from internal work of the industrial partner. It is envisioned that the majority of the data used for training of this framework will be based on available data, with additional computations carried out only when required, to extend the dataset for wider generalisability.

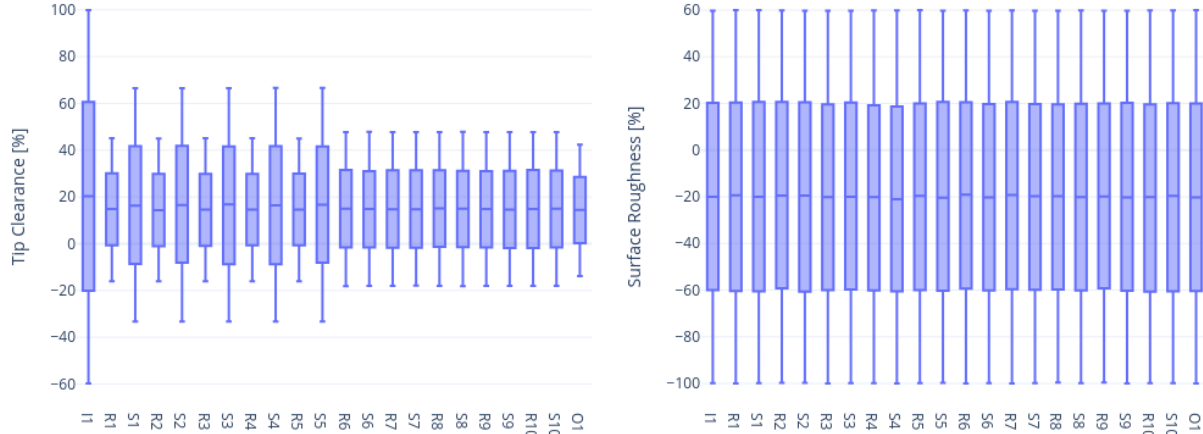


Figure 2: Box plots of the input variables (tip clearance and surface roughness) at each blade row

The CFD results are processed to only extract six variables, namely, Total Pressure (P_t), Total Temperature (T_t), Axial Velocity (V_x), Tangential Velocity (V_t), Radial Velocity (V_r), and Density (ρ), at each of the 24 inter-row locations as shown in Figure 1. The flow condition at each mesh node is fully described by the six variables and can be used to calculate all other available flow variables in the CFD solution. While the CFD mesh for each simulation comprises over 15 million nodes, the post-processed domain contains less than 100 thousand nodes overall, yet it includes all the necessary information for the desired engineering assessment. This consists only of the 24 inter-row 2D planes with a 64×64 grid. The data is stored as a tensor with a channel-first convention and a shape of $(6 \times 24 \times 64 \times 64)$, where the dimensions represent the number of variables, number of axial locations, tangential

nodes in the mesh, and radial nodes in the mesh, respectively. To reduce the computational cost of the CFD analysis, rotational periodicity can be assumed, and only a single passage needs to be considered instead of the full annulus, as standard process for steady state CFD analysis. However, when generating single passage meshes, the location of the periodic boundaries can vary depending on the meshing approach or geometry. As the methodology aims to be generalisable, the data is interpolated for a given passage at a fixed circumferential location defined in the CFD post-processing step, irrespective of the periodic boundary definitions in the mesh. This is appropriate as the geometry definitions considered have a specific clocking configuration, and all the manufacturing and build variations are imposed based on it. This allows to obtain 2D contours which are not limited to a given mesh or geometry, as typical in most surrogate models developed for optimisations. However, 2D contours are only used for detailed analyses, whereas mass-flow averaging [24] in the circumferential direction is more commonly used to obtain radial profiles of the variables of interest for most engineering applications. These radial profiles of each variable are then mass-flow averaged [24] to obtain a 1D average, which is used to calculate stage-wise performance of the variables of interest, such as pressure-ratio (PR), and polytropic efficiency (η_p). In addition to the aerodynamic performance of the stage, it is possible to calculate the overall performance of the compressor. Predicting the stage-wise performance in addition to the overall performance is critical for implementation of the model in the gas turbine build process, as it provides detailed information on which blade rows should be targeted by corrective measures.

2.2. The $C(NN)FD$ framework

The tip clearance and surface roughness values, as well as the relevant geometry design parameters of a specific build are fed as input to $C(NN)FD$, which predicts the 2D contours for all variables at the locations of interest. The outputs are mass-flow averaged to obtain the relevant radial profiles and 1D averages, which are then used to calculate stage-wise performance first, and then the overall performance using relevant thermodynamic equations. As the impact of tip clearance and surface roughness variations depends on the aerodynamic loading distribution of a given aerofoil, the methodology should be generalisable to different designs. Therefore, $C(NN)FD$ requires the geometries associated with each clearance value as input. This is achieved by considering a series of design parameters to describe the geometry of each blade, such as stagger angle, camber angle, maximum thickness, etc. Since we consider only a single compressor design, the geometry parameters are fixed. In future work we will investigate the effect of geometrical variations and different designs.

2.2.1. Pre-processing

The input of the network consists of two separate tensors. The first input is a tensor of size (2×22) , where the dimensions represent the input variables for each airfoil, respectively tip clearance and surface roughness, and the number of blade rows in the compressor. The second input is a tensor of size $(5 \times 22 \times 8)$ with the blade geometry design parameters. The dimensions represent the number of design variables, number of rows and number of radial sections. The compressor consists of 22 blade-rows, and aim of the network is to predict the flow field downstream of each of these blade-rows, at the corresponding 22 inter-row locations. However, for compressor aerodynamic analysis, often two additional locations are considered to calculate the overall performance: "Compressor Inlet" and "Compressor Outlet", respectively upstream of the first row and downstream of the last row. This brings the number of axial locations for the predictions to 24. Therefore, the input tensor is manipulated by duplicating the input data for the first row at the beginning of the tensor, and the input data for the last row at the end of the tensor, bringing the first dimension of the tensor to 24. The input geometry tensor includes 8 radial sections at which the design parameters are specified, but this number can vary depending on the aerodynamic design philosophy for the compressor design of interest. Therefore, the radial sections are interpolated to computational grid, bringing input geometry shape to $(5 \times 24 \times 64)$. The geometry definition is then copied in the tangential direction to match the computational grid, defining a tensor of shape $(5 \times 24 \times 64 \times 64)$. Likewise, the input tensor containing the tip clearance and surface roughness variables of shape (2×24) is copied in the radial and tangential direction, to give a tensor of shape $(2 \times 24 \times 64 \times 64)$. This allows to map the 2D and 3D input tensors to the 4D output tensor required for the flow field predictions. The two tensors are then added, resulting in a $(7 \times 24 \times 64 \times 24)$ tensor, using a channel first convention. The number of channels is now representative of the input variables, including: tip clearance, surface roughness, inlet metal angle, outlet metal angle, maximum thickness, chord and pitch. The number of input variables could increase if considering more manufacturing and build variations. Therefore, a convolution is adopted to change

the number of channels from the number of input design variables, to the number of output flow variables, which in this instance is 6. This results in a tensor of shape $(6 \times 24 \times 64 \times 64)$ matching the requirements for the output flow field predictions. If more variables were required for the flow field predictions, it would only be required to extract the relevant data from the CFD solution and to increase the number of channels accordingly.

2.2.2. Neural Network architecture

The architecture shown in Figure 3, is a variant of the one originally proposed by the authors in previous work [4]. Following a pre-processing step for the input variables, the model is based on a 3D U-Net architecture with double residual convolutional blocks. Each convolutional block consists of a 3D convolution layer, followed by batch normalization and an *ELU* activation function. A residual connection is implemented from after the first convolution to before the second activation function. The use of residual connections improves convergence and makes this type of architecture scalable to larger models required for full compressor applications. The number of axial locations is fixed to 24, and each down-sampling convolutions and up-sampling transposed convolutions uses a stride of $(1, 2, 2)$, resulting in a bottleneck section with tensors of shape $(384 \times 24 \times 1 \times 1)$ after six layers. Both up and down samplings are followed by a double convolutional block at each layer. The output of the network is a tensor of size $(6 \times 24 \times 64 \times 64)$, which encompasses the entire flow field. The encoding section followed by the decoding section, along with the skip connections, enables the network to predict both low-level and high-level features in the flow field.

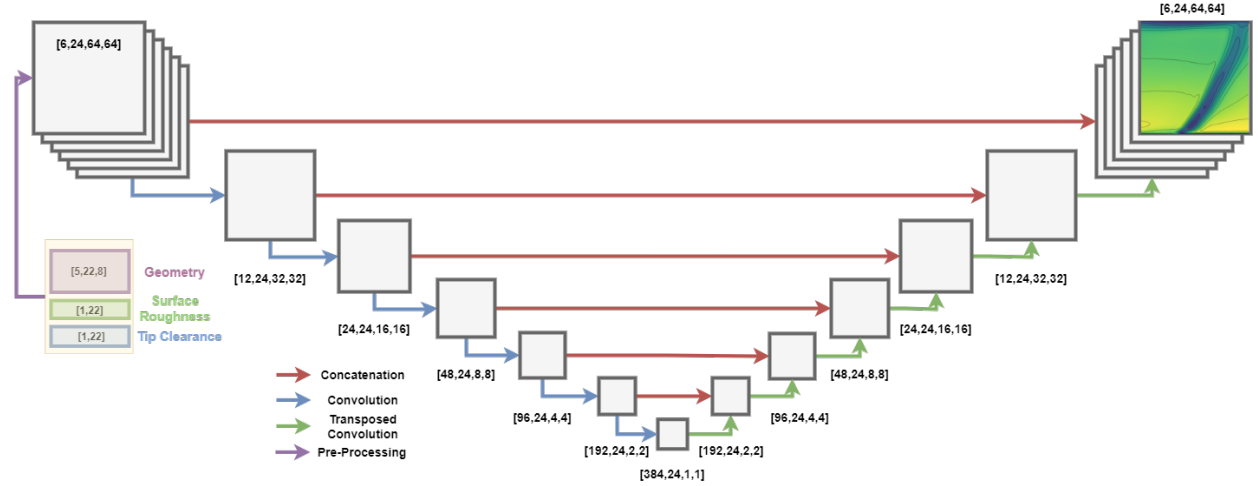


Figure 3: C(NN)FD architecture overview

2.2.3. Training

The network is trained using the *AdamW* optimizer, with *Huber* loss function. The dataset was divided into three sets: 70% training data, 20% validation data, and 10% hold-out data. The validation set was utilized to evaluate model performance and perform hyper-parameter tuning, while the hold-out set was reserved only for a final assessment. This ensures that the results are generalisable to unseen cases, and will lead to comparable performance also when deployed in a production environment. The dataset is split in a stratified manner, dividing the data in 10 bins using a quantile-based discretization function on the target overall efficiency. This ensures that each dataset has a comparable distribution. It should be noted that the dataset already contains out-of-tolerance cases and that no further out-of-distribution data outside of those limits is expected for the engineering application of interest. For further robustness, the training is performed using 5 different values of the random seed used for the dataset split, batch selection and initialization. The results are then presented providing the mean and the standard deviation of the losses. For instance, the final model showed a training loss of $(1.29 \pm 0.16) \cdot 10^{-3}$ and a test loss of $(1.96 \pm 0.40) \cdot 10^{-3}$ (Huber Loss \pm standard deviation). An example of the training curve for one seed, starting from a random initialization is shown in Figure 4. The training runs generally converged within 500 epochs, with a batch size of 20 and an initial learning rate of 0.01. A learning rate scheduler was implemented, which halved the learning rate with a patience of 20 epochs. To

avoid overfitting, early stopping with a patience of 50 epochs was implemented. The training time for a new model from scratch is around 3 hours on a single Tesla K80 GPU. This is reduced to less than 1 hour when re-training the network when data becomes available, thus making the architecture scalable for industrial applications. The execution time for inference is less than 1 second, making the predictions of the deployed model effectively real-time for the application of interest.

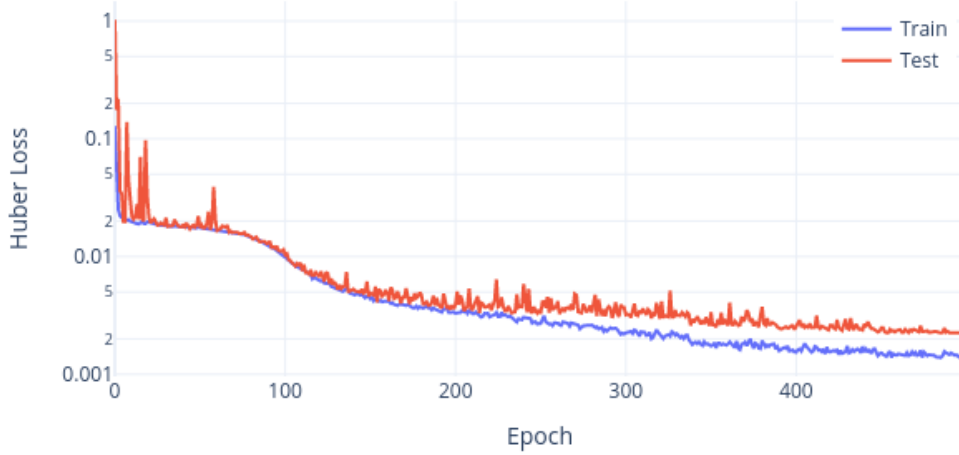


Figure 4: Training history: Training loss and Test loss

2.2.4. Model Comparison

The novelty of the $C(NN)FD$ framework has been discussed in Section 1.4, highlighting how the appropriate pre-processing of the CFD solution and the usage of the relevant physical equations allow for the usage of CNNs for flow field predictions of complex 3D turbomachinery flows. However, the complexity of the regression problem will increase with the number of input features considered, due for example to: number of stages in the compressor and associated geometry parametrization, manufacturing variations considered (tip clearance, surface roughness, geometry variations or more) and operating conditions. Therefore, the complexity of the machine learning problem distinguishes this work from similar ones in literature [4]. For comparison, three different machine learning models are considered. The first one, *Double Convolution* consists only two convolution layers, each of which with 3D convolution, batch normalization, and ELU activation function. The second model, *Standard U-Net* is a 3D implementation of the U-Net, comparable to the ones used in previous literature for 2D airfoil flow predictions [13]. The $C(NN)FD$ is the architecture presented in this paper, and discussed in more details in Section 2.2.2. The main difference between the last two is that $C(NN)FD$ includes residual connections within the double convolution blocks. Moreover, *Standard U-Net* uses a constant stride of (2, 2, 2) across the three dimensions when downsampling and upsampling, which due to the target size of $(6 \times 24 \times 64 \times 64)$ limits the width of the U-Net to three layers. In $C(NN)FD$ the number of axial locations is instead fixed to 24 by using a stride of (1, 2, 2), which allows for a wider U-Net with a total of six layers. The test loss of *Double Convolution* is $10.3x$ higher than $C(NN)FD$, while *Standard U-Net* is $3.28x$ higher. The accuracy achieved by these two architectures would not be sufficient to be used for the engineering application of interest. The improved accuracy of $C(NN)FD$ is due to the higher number of trainable parameters and computational cost for $C(NN)FD$. However, more complex models such as U-Net++ [25] did not lead to an improvement in the accuracy of the predictions. Regardless, they will be considered in future work for more complex datasets, such as the ones including also geometrical variations or different operating conditions.

Table 1: Model comparison and benchmarking for different CNN architectures

Model	Trainable Parameters	Wall Time [h]	Train Loss	Test Loss
<i>Double Convolution</i>	$5.22 \cdot 10^3$	0.8	$17.39 \cdot 10^{-3}$	$17.85 \cdot 10^{-3}$
<i>Standard U-Net</i> [13]	$3.19 \cdot 10^5$	2.3	$5.40 \cdot 10^{-3}$	$5.67 \cdot 10^{-3}$
<i>C(NN)FD</i>	$1.28 \cdot 10^7$	3.6	$1.26 \cdot 10^{-3}$	$1.73 \cdot 10^{-3}$

3. Results

In this section, the predicted flow field generated by *C(NN)FD* is compared to the CFD ground truth for the worst case scenario, where the largest discrepancy between the two was found in the hold-out set. A comparison between the ground truth on the left and the predictions on the right provides an overview of the flow field differences. The results are presented for Axial Velocity V_x in Figure 5, Figure 6 and Figure 7 at Stage-1, Stage-5 and Stage-10. The relative error between the ground truth and the predictions at each mesh node are shown in Figure 8, Figure 9 and Figure 10 for Axial Velocity V_x at Stage-1, Stage-5, and Stage-10. All the other stages and variables exhibit similar level of agreement and are not presented for conciseness.

All values presented are non-dimensionalized with respect to the results obtained from the baseline. The *Span [%]* y-axis represents the radial direction in the gas path, ranging from the hub surface at the bottom to the casing surface at the top. The *θ [%]* x-axis represents the circumferential direction in the gas path, with a range between 0 and 1 representing one passage. Each row corresponds to a specific number of blades, and thus the gas path can be divided into a number of passages equal to the blade count. The predictions generated by *C(NN)FD* exhibit excellent agreement with the ground truth, with the primary flow features being accurately reproduced. Only minor differences are observed in regions with high gradients, but well within the numerical uncertainty of the CFD solver. Due to operational requirements, the aerodynamic design of axial compressor leads to greatly different flow features across the different stages. For instance, front stages tend to operate at transonic conditions, with strong shock-waves interacting with the tip leakage flows. Conversely, the rear stages are subsonic, with the flow field dominated by end-wall flow features. The proposed architecture is demonstrated to be able to predict the flow field within the compressor for both transonic and subsonic stages, even with significantly different flow features as seen for instance by comparing Figure 5 and Figure 7. The highest local error is in the order of magnitude of 0.1%, which is well within the numerical error of the CFD solver. The errors are generally localised to regions with steep gradients and to only few nodes in the mesh, being therefore effectively negligible from an engineering perspective. When performing mass-flow averaging to obtain the radial profiles, the discrepancies between the ground truth and predictions are even less significant. Figure 11, Figure 12 and Figure 13 indicate that the radial profiles for *C(NN)FD* and CFD are effectively overlapping. The results are presented for Stage-1, Stage-5 and Stage-10. All the other stages and variables exhibit similar level of agreement and are not presented for conciseness. It is notable how even the end-wall regions, characterized by steep gradients, are well-resolved by *C(NN)FD*. This confirms that the localized errors found in the 2D contours prediction do not significantly affect the results for the radial profiles.

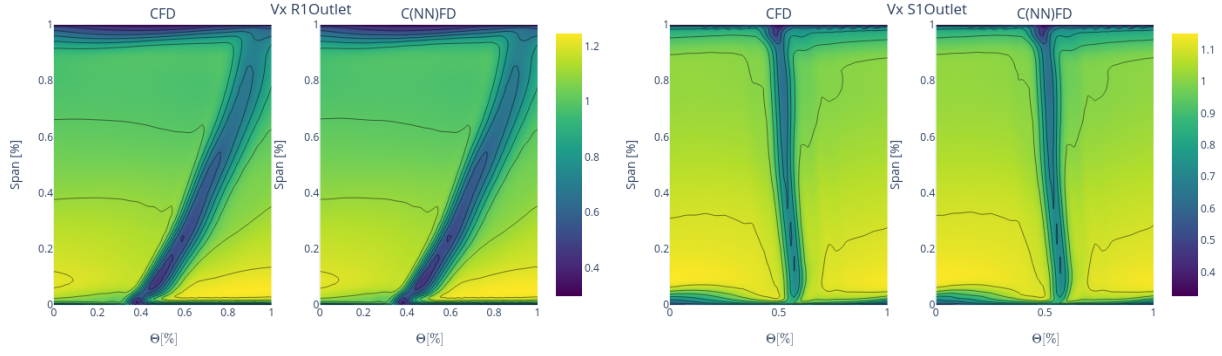


Figure 5: V_x contour comparison between CFD and C(NN)FD predictions: Stage 1 - Rotor outlet and Stator outlet

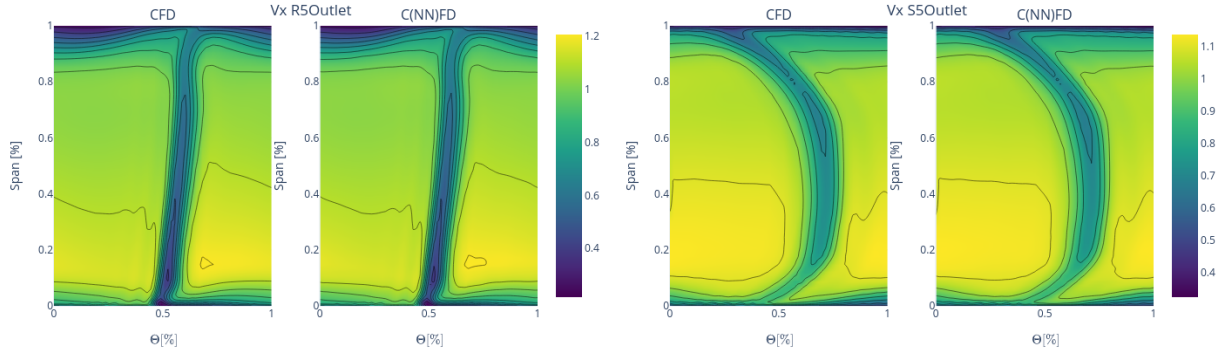


Figure 6: V_x contour comparison between CFD and C(NN)FD predictions: Stage 5 - Rotor outlet and Stator outlet

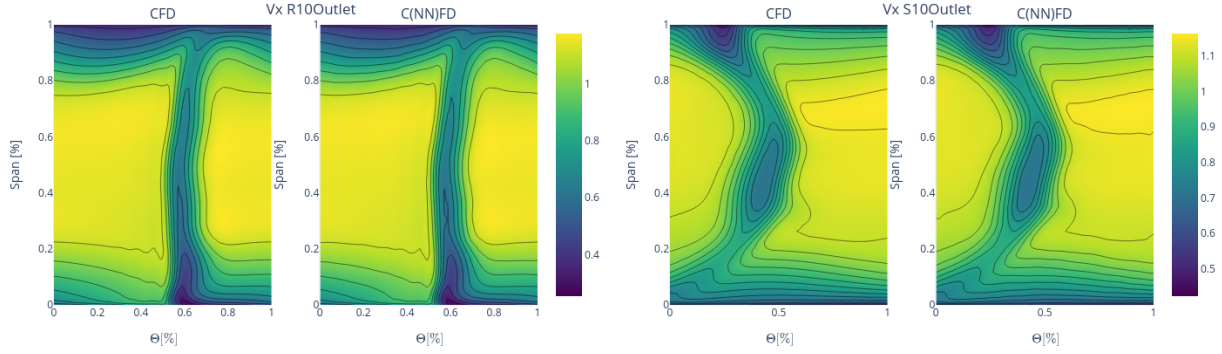


Figure 7: V_x contour comparison between CFD and C(NN)FD predictions: Stage 10 - Rotor outlet and Stator outlet

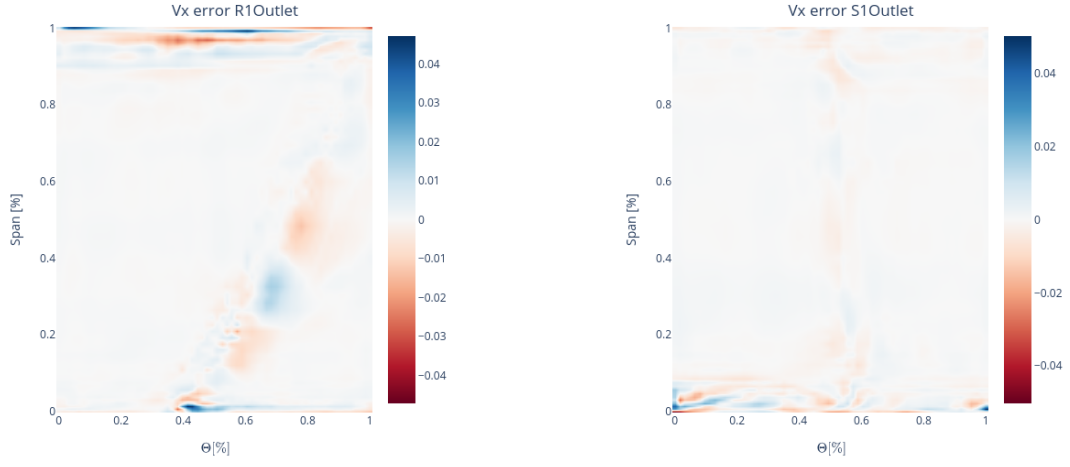


Figure 8: V_x error comparison between CFD and C(NN)FD predictions: Stage 1 - Rotor outlet and Stator outlet

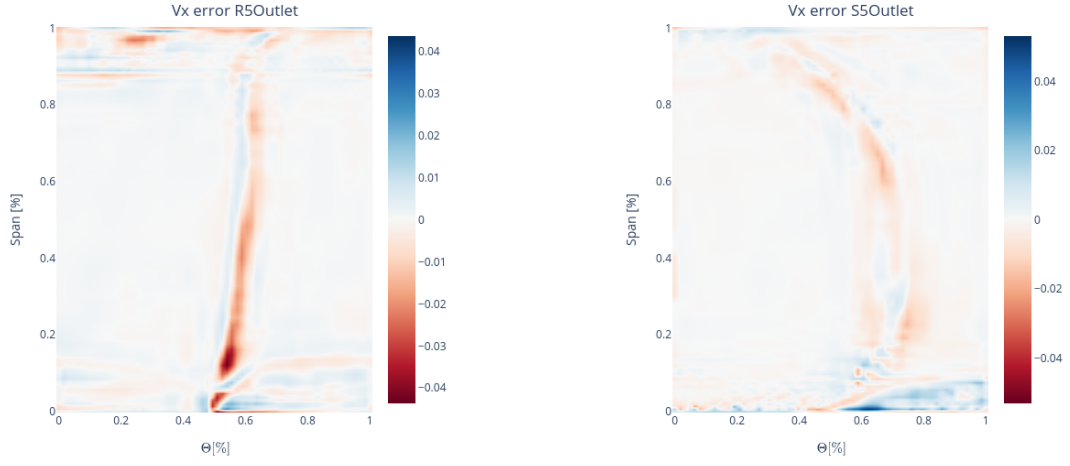


Figure 9: V_x error comparison between CFD and C(NN)FD predictions: Stage 5 - Rotor outlet and Stator outlet

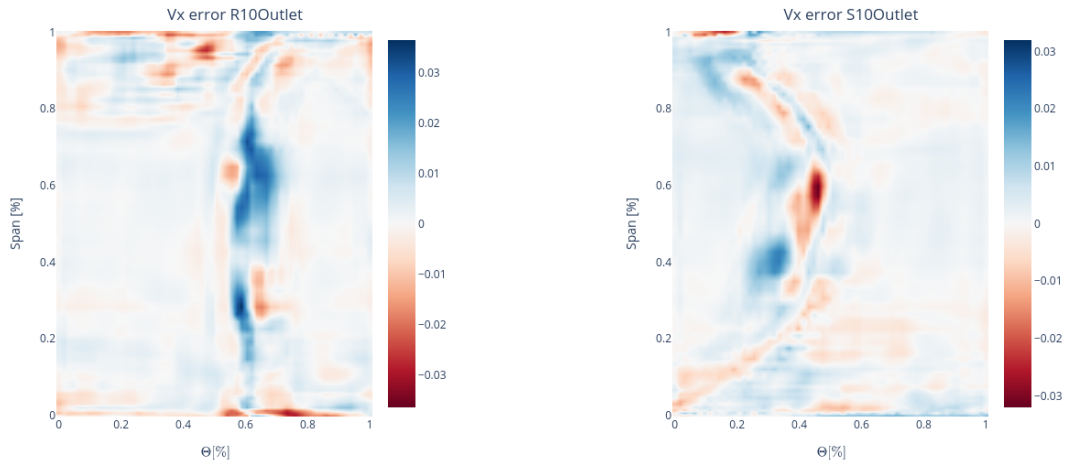


Figure 10: V_x error comparison between CFD and C(NN)FD predictions: Stage 10 - Rotor outlet and Stator outlet

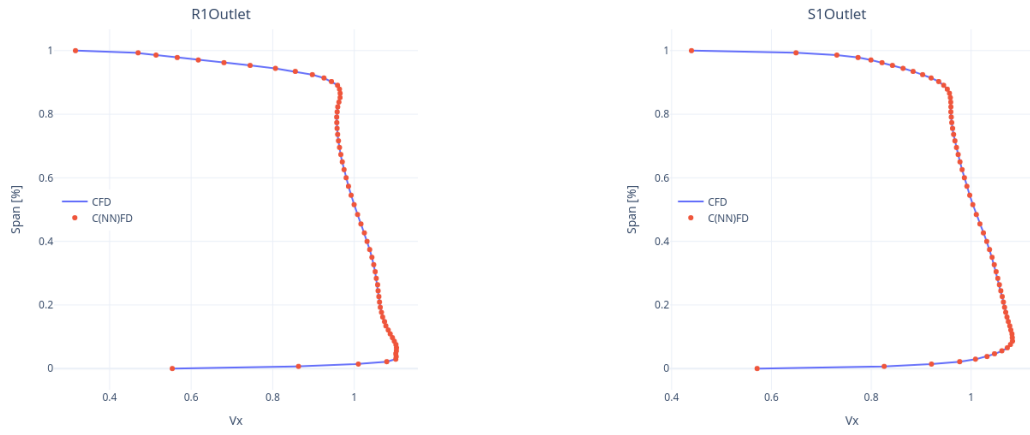


Figure 11: Radial profiles comparison between CFD and C(NN)FD predictions: Stage 1 - Rotor outlet and Stator outlet

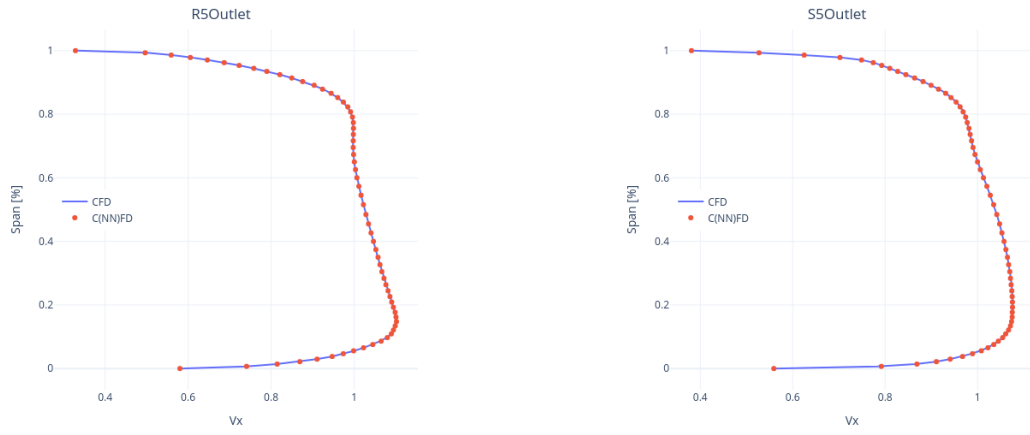


Figure 12: Radial profiles comparison between CFD and C(NN)FD predictions: Stage 5 - Rotor outlet and Stator outlet

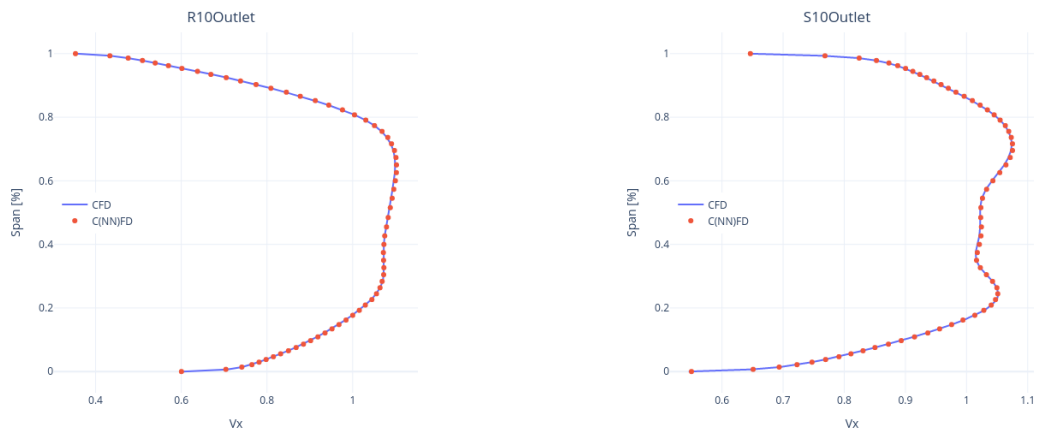


Figure 13: Radial profiles comparison between CFD and C(NN)FD predictions: Stage 10 - Rotor outlet and Stator outlet

The radial profiles are then mass-flow averaged to obtain the relevant 1D averages. An overview of the 1D average at each inter-row location is shown for Total Pressure P_t in Figure 14a, Total Temperature T_t in Figure 14b, Axial Velocity V_x in Figure 14c and Density ρ in Figure 14d. Only these variables are presented as required to calculate the stage-wise and overall performance. However, similar agreement was also found for the remaining variables.



Figure 14: Row-wise distributions comparison between predicted (C(NN)FD) and ground truth (CFD) values for worst case in the hold-out set

The 1D averages are then utilized to compute the stage-wise performance as shown in Figure 15a. Predicting the stage-wise performance in addition to the overall performance is critical for implementation of the model in the gas turbine build process, as it provides detailed information on which blade rows should be targeted by corrective measures. While the agreement is excellent, minor discrepancies between predictions and ground truth are noticeable. C(NN)FD predicts accurately the trend for each stage, relative to the baseline, with the variations being slightly over-predicted or under-predicted depending on the stage. The large drop in Stage-10 efficiency could also potentially affect the compressor exit diffuser performance, which will also be considered in future work.

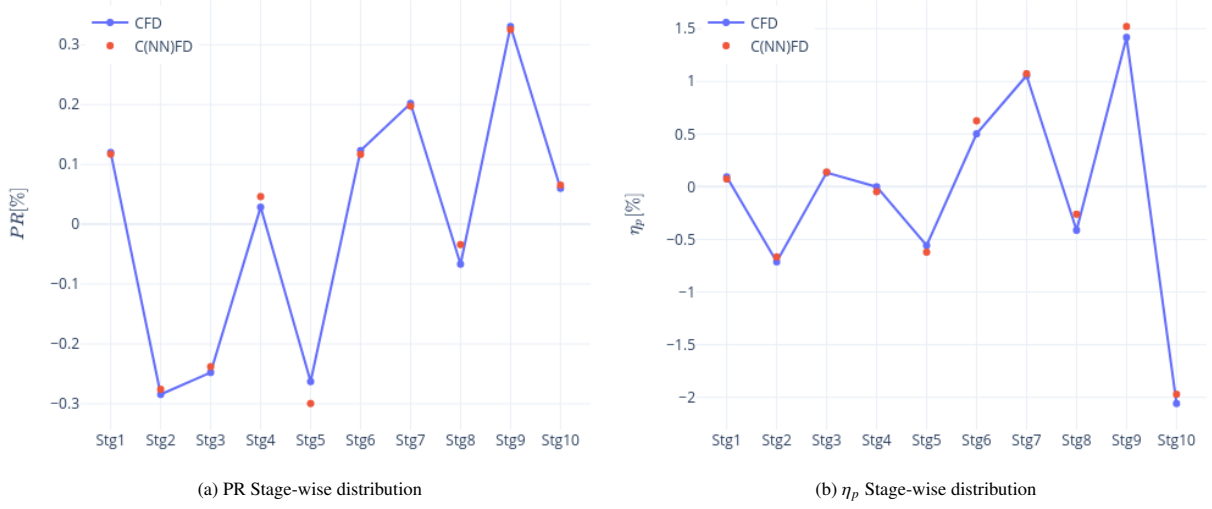


Figure 15: Comparison between predicted (C(NN)FD) and ground truth (CFD) values for worst case in the hold-out set

The overall performance predictions are presented in Table 2, Figure 16a and Figure 16b. An excellent agreement is observed for all overall performance parameters, with a coefficient of determination R^2 close to 1 for all variables. This indicates that the proposed model can accurately describe most of the variance present in the dataset. Moreover, the Mean-Absolute-Error for each variable is smaller than the known uncertainties of the CFD ground truth results and significantly smaller than the dataset's range. If required, the predictions could potentially be further improved by providing training data including more extreme conditions, where it was deemed relevant from an industrial perspective.

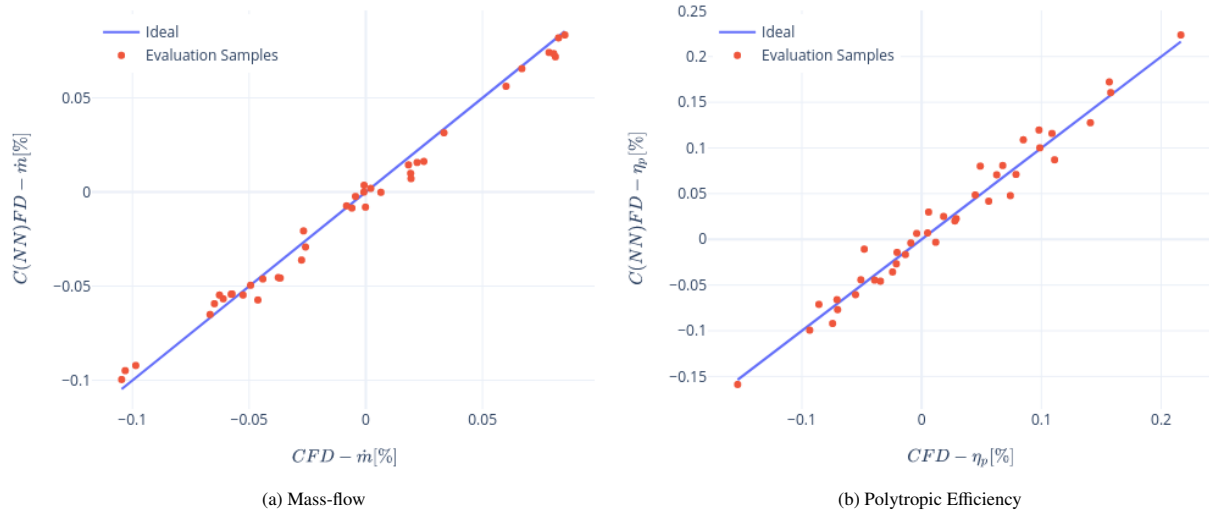


Figure 16: Comparison between predicted (C(NN)FD) and ground truth (CFD) values

Table 2: Overall performance comparison

Var	R^2	MAE%	$\Delta dataset\%$
\dot{m}	0.987	0.004	0.25
η_p	0.968	0.011	0.47

The $C(NN)FD$ predictions remain accurate even for the case with the lowest efficiency in the hold-out set, demonstrating the model’s capability to handle challenging aerodynamic conditions typical of large clearances and surface roughness. The largest discrepancy shows a difference of less than 0.05 percentage points in overall efficiency. This discrepancy is negligible for overall performance predictions, and demonstrates how the proposed architecture reliably predicts even the most challenging cases. This is a particularly challenging case aerodynamically, as high and low efficiency and pressure ratio stages are alternated, as shown in Figure 15b . This would result for example in strong tip leakage flows leading to high losses and low efficiency in the blade rows with large clearances. Those would affect the downstream blade rows with tight clearance, whose potentially high efficiency will be affected by the unfavorable upstream conditions, leading to complex inter-row interactions and stage re-matching. This demonstrates how $C(NN)FD$ can be used as a predictive tool to assess the performance of a given engine build, without the need for computationally expensive CFD analysis, and potentially avoiding re-testing for engines which would not meet the contractual performance requirements. Moreover, this tool can be used for a selective build process, where different parts available in stock can be selected based on the expected overall performance. The focus of this work was on compressor performance at design points conditions, while future work will extend the assessment to more off-design conditions and surge margin predictions.

4. Conclusion

This study presents the development and application of a novel deep learning framework for real-time predictions of the impact of tip clearance variations on the flow field and overall performance of multi-stage axial compressors. The proposed $C(NN)FD$ architecture achieves real-time accuracy comparable to the CFD benchmark. Our methodology is generalisable because of the flow field predictions, which are utilized to calculate using the relevant physical equations the corresponding radial profiles, 1D averages, stage-wise distributions and overall performance. Our methodology is demonstrated to be scalable to industrial applications because of physics-based selective use of relevant parts of the CFD solution. The deployed model, is readily integrated within the manufacturing and build process of gas turbines, thus providing the opportunity to analytically assess the impact on performance and to take the appropriate measures to potentially avoid repeating expensive physical tests and CO_2 emissions.

5. Acknowledgements

The authors would like to thank Siemens Energy Industrial Turbomachinery Ltd. for allowing the publication of this research, as well as Richard Bluck and Roger Wells for their support and comments. This work was supported and funded by Siemens Energy Industrial Turbomachinery Ltd.

References

- [1] G. Bruni, S. K. Krishnababu, Manufacturing and build variations modelling for multi-stage axial compressors: Cfd aerodynamic predictions, no. GT2024-122636, 2024. doi:10.1115/GT2024-122636.
- [2] F. Montomoli, Uncertainty quantification in computational fluid dynamics and aircraft engines: Second edition, Springer International Publishing, 2018. doi:10.1007/978-3-319-92943-9. URL <https://doi.org/10.1007/978-3-319-92943-9>
- [3] J. Wang, X. Zheng, Review of Geometric Uncertainty Quantification in Gas Turbines, Journal of Engineering for Gas Turbines and Power 142 (7) (06 2020). doi:10.1115/1.4047179. URL <https://doi.org/10.1115/1.4047179>
- [4] G. Bruni, S. Maleki, S. K. Krishnababu, $C(nn)fd$ - a deep learning framework for turbomachinery cfd analysis (2023). arXiv:2306.05889.
- [5] J. A. Storer, N. A. Cumpsty, Tip Leakage Flow in Axial Compressors, Journal of Turbomachinery 113 (2) (1991) 252–259. doi:10.1115/1.2929095. URL <https://doi.org/10.1115/1.2929095>

- [6] S. Sakulkaew, C. S. Tan, E. Donahoo, C. Cornelius, M. Montgomery, Compressor Efficiency Variation With Rotor Tip Gap From Vanishing to Large Clearance, *Journal of Turbomachinery* 135 (3) (03 2013). doi:10.1115/1.4007547.
URL <https://doi.org/10.1115/1.4007547>
- [7] V. Suriyanarayanan, Q. Rendu, M. Vahdati, L. Salles, Effect of Manufacturing Tolerance in Flow Past a Compressor Blade, *Journal of Turbomachinery* 144 (4) (11 2021). doi:10.1115/1.4052600.
URL <https://doi.org/10.1115/1.4052600>
- [8] S. Krishnababu, O. Valero, R. Wells, AI Assisted High Fidelity Multi-Physics Digital Twin of Industrial Gas Turbines, Vol. Volume 2D of Turbo Expo: Power for Land, Sea, and Air, 2021. doi:10.1115/GT2021-58925.
URL <https://doi.org/10.1115/GT2021-58925>
- [9] J. Pongetti, T. Kipouros, M. Emmanuelli, R. Ahlfeld, S. Shahpar, Using Autoencoders and Output Consolidation to Improve Machine Learning Models for Turbomachinery Applications, Vol. Volume 2D of Turbo Expo: Power for Land, Sea, and Air, 2021. doi:10.1115/GT2021-60158.
URL <https://doi.org/10.1115/GT2021-60158>
- [10] G. Bruni, S. Krishnababu, S. Jackson, Application of Machine Learning to Forced Response Predictions of an Industrial Axial Compressor Rotor Blade, *Journal of Engineering for Gas Turbines and Power* 145 (1) (10 2022). doi:10.1115/1.4055634.
URL <https://doi.org/10.1115/1.4055634>
- [11] X. He, M. Rauseo, Q. Rendu, L. Salles, M. Vahdati, F. Zhao, Turbomachinery aerodynamic and aeroelastic predictions with machine learning, 16th International Symposium on Unsteady Aerodynamics Aeroacoustics and Aeroelasticity of Turbomachines, 2022.
- [12] N. Thuerey, K. Weissenow, L. Prantl, X. Hu, Deep learning methods for reynolds-averaged navier-stokes simulations of airfoil flows (10 2018). doi:10.2514/1.j058291.
URL <http://arxiv.org/abs/1810.08217><http://dx.doi.org/10.2514/1.j058291>
- [13] N. Thuerey, K. Weissenow, L. Prantl, X. Hu, Deep learning methods for reynolds-averaged navier-stokes simulations of airfoil flows, *AIAA Journal* 58 (1) (2020) 25–36. doi:10.2514/1.J058291.
URL <https://doi.org/10.2514/1.J058291>
- [14] M. D. Ribeiro, A. Rehman, S. Ahmed, A. Dengel, Deepcfd: Efficient steady-state laminar flow approximation with deep convolutional neural networks (4 2020).
URL <http://arxiv.org/abs/2004.08826>
- [15] A. Kashefi, D. Rempe, L. J. Guibas, A point-cloud deep learning framework for prediction of fluid flow fields on irregular geometries, *Physics of Fluids* 33 (2) (02 2021). doi:10.1063/5.0033376.
URL <https://doi.org/10.1063/5.0033376>
- [16] N. Li, J. Winkler, C. A. Reimann, D. Voytovych, M. Joly, K. G. Lore, J. Mendoza, S. M. Grace, Machine learning aided fan broadband interaction noise prediction for leaned and swept fans, in: *AIAA AVIATION 2023 Forum*. doi:10.2514/6.2023-4297.
URL <https://arc.aiaa.org/doi/abs/10.2514/6.2023-4297>
- [17] A. N. Rao, S. C. Stapelfeldt, A. Duncan, S. Shahpar, F. Montomoli, Towards real-time cfd, *ECCOMAS*, 2023, pp. 180–188. doi:10.7712/140123.10198.18946.
- [18] L. Harsch, S. Riedelbauch, Direct prediction of steady-state flow fields in meshed domain with graph networks, *International Conference on Learning Representations*, 2021.
URL <https://doi.org/10.48550/arXiv.2105.02575>
- [19] T. Pfaff, M. Fortunato, A. Sanchez-Gonzalez, P. Battaglia, Learning mesh-based simulation with graph networks, *International Conference on Learning Representations*, 2021.
URL <https://doi.org/10.48550/arXiv.2010.03409>
- [20] K. Beqiraj, A. Perrone, M. Sanguineti, L. Ratto, G. Ricci, Rotor37 Aerodynamic Optimization: A Machine Learning Approach, Vol. Volume 10D of Turbo Expo: Power for Land, Sea, and Air, 2022. doi:10.1115/GT2022-83063.
URL <https://doi.org/10.1115/GT2022-83063>
- [21] J. Li, T. Liu, Y. Wang, Y. Xie, Integrated graph deep learning framework for flow field reconstruction and performance prediction of turbomachinery, *Energy* 254 (2022) 124440. doi:https://doi.org/10.1016/j.energy.2022.124440.
URL <https://doi.org/10.1016/j.energy.2022.124440>
- [22] N. Thuerey, P. Holl, M. Mueller, P. Schnell, F. Trost, K. Um, Physics-based Deep Learning, *WWW*, 2021.
URL <https://physicsbaseddeeplearning.org>
- [23] M. Chu, N. Thuerey, H.-P. Seidel, C. Theobalt, R. Zayer, Learning meaningful controls for fluids, *ACM Trans. Graph.* 40 (4) (jul 2021). doi:10.1145/3450626.3459845.
URL <https://doi.org/10.1145/3450626.3459845>
- [24] N. A. Cumpsty, J. H. Horlock, Averaging Nonuniform Flow for a Purpose, *Journal of Turbomachinery* 128 (1) (2005) 120–129. doi:10.1115/1.2098807.
URL <https://doi.org/10.1115/1.2098807>
- [25] Z. Zhou, M. M. R. Siddiquee, N. Tajbakhsh, J. Liang, Unet++: A nested u-net architecture for medical image segmentation (7 2018).
URL <http://arxiv.org/abs/1807.10165>